



Ultrasensitive detection of cancer biomarkers by nickel-based isolation of polydisperse extracellular vesicles from blood

Michela Notarangelo^a, Chiara Zucal^a, Angelika Modelska^a, Isabella Pesce^b, Giordina Scarduelli^c, Cristina Potrich^d, Lorenzo Lunelli^d, Cecilia Pederzoli^d, Paola Pavan^e, Giancarlo la Marca^f, Luigi Pasini^g, Paola Ulivi^g, Himisha Beltran^h, Francesca Demichelis^a, Alessandro Provenzani^{a,1}, Alessandro Quattrone^{a,1}, Vito G. D'Agostino^{a,*,1}

^a Department of Cellular, Computational and Integrative Biology (CIBIO), University of Trento, Via Sommarive 9, Trento 38123, Italy

^b Cell Analysis and Separation Core Facility (CIBIO), University of Trento, Via Sommarive 9, Trento 38123, Italy

^c Advanced Imaging Core Facility (CIBIO), University of Trento, Via Sommarive 9, Trento 38123, Italy

^d Fondazione Bruno Kessler (FBK), Laboratory of Biomolecular Sequence and Structure Analysis for Health, Trento, Via Sommarive 14, Trento 38123, Italy

^e Immunohematology and Cell Factory Unit, Meyer Children's University Hospital, Viale Pieraccini 24, Florence 50139, Italy

^f Department of Experimental and Clinical Biomedical Sciences, Centro di Eccellenza Denoche, Aou Meyer University of Florence, Viale Pieraccini 6, 50139, Italy

^g Istituto Scientifico Romagnolo per lo Studio e la Cura dei Tumori (IRST) IRCCS, Via Piero Maroncelli 40, Meldola 47014, Italy

^h Department of Medical Oncology, Dana Farber Cancer Institute, Boston, MA, USA

ARTICLE INFO

Article history:

Received 18 January 2019

Received in revised form 6 April 2019

Accepted 18 April 2019

Available online 29 April 2019

Keywords:

Cancer
 Biomarkers
 Extracellular vesicles
 Liquid biopsy
 Nickel
 Alpha
 Droplet PCR

ABSTRACT

Background: Extracellular vesicles (EVs) are secreted membranous particles intensively studied for their potential cargo of diagnostic markers. Efficient and cost-effective isolation methods need to be established for the reproducible and high-throughput study of EVs in the clinical practice.

Methods: We designed the nickel-based isolation (NBI) to rapidly isolate EVs and combined it with newly-designed amplified luminescent proximity homogeneous assay or digital PCR to detect biomarkers of clinical utility.

Findings: From plasma of 46 healthy donors, we systematically recovered small EV (~250 nm of mean diameter; $\sim 3 \times 10^{10}/\text{ml}$) and large EV (~560 nm of mean diameter; $\sim 5 \times 10^8/\text{ml}$) lineages ranging from 50 to 700 nm, which displayed hematopoietic/endothelial cell markers that were also used in spike-in experiments using EVs from tumor cell lines. In retrospective studies, we detected picomolar concentrations of prostate-specific membrane antigen (PSMA) in fractions of EVs isolated from the plasma of prostate cancer patients, discriminating them from control subjects. Directly from oil-encapsulated EVs for digital PCR, we identified somatic *BRAF* and *KRAS* mutations circulating in the plasma of metastatic colorectal cancer (CRC) patients, matching 100% of concordance with tissue diagnostics. Importantly, with higher sensitivity and specificity compared with immuno-isolated EVs, we revealed additional somatic alterations in 7% of wild-type CRC cases that were subsequently validated by further inspections in the matched tissue biopsies.

Interpretation: We propose NBI-combined approaches as simple, fast, and robust strategies to probe the tumor heterogeneity and contribute to the development of EV-based liquid biopsy studies.

Fund: Associazione Italiana per la Ricerca sul Cancro (AIRC), Fondazione Cassa di Risparmio Trento e Rovereto (CARITRO), and the Italian Ministero Istruzione, Università e Ricerca (Miur).

© 2019 The Authors. Published by Elsevier B.V. This is an open access article under the CC BY-NC-ND license (<http://creativecommons.org/licenses/by-nc-nd/4.0/>).

1. Introduction

Extracellular vesicles (EVs) are membranous particles, composed of a lipid bilayer, that are massively secreted in biological fluids, where they are involved in cell-to-cell communication [1–3]. According to different mechanisms of biogenesis [4], EVs are classified into exosomes and microvesicles (or ectosomes), derivatives of the endosomal system or produced by outward budding of the plasma membrane, respectively

* Corresponding author at: Department of Cellular, Computational and Integrative Biology (CIBIO), University of Trento, Via Sommarive 9, Trento 38123, Italy.

E-mail addresses: himisha_beltran@dfci.harvard.edu (H. Beltran),

vito.dagostino@unitn.it (V.G. D'Agostino).

¹ Co-last authors.

Research in context

Evidence before this study

The abundance and biological content of heterogeneous EVs in biological fluids qualify them as an attractive source of diagnostic markers. However, reproducible and efficient isolation methods need to be established for application in clinical practice. Rapid approaches that minimize protein contaminants exploited the surface charge of EVs to capture them.

Added value of this study

We designed a rapid and cost-effective procedure to obtain EVs in a physiological pH solution, while preserving vesicles' integrity/stability and minimizing particle aggregation. We exploited these advantages to combine this approach with highly sensitive immobilization-independent assays to detect cancer biomarkers, i.e. specific proteins or RNA species present in EVs. We show that a comprehensive isolation of EVs offers a strategic advantage for detecting tumor biomarkers from liquid biopsy.

Implications of all the available evidence

This study indicates the possibility of detecting, from circulating EVs, rare somatic alterations in driver genes that mirror the heterogeneity of tumor cells present in the matched tissue biopsies.

[4]. EVs are highly heterogeneous in size and molecular composition [5]: exosomes are generally smaller than 150 nm and microvesicles can overlap to some extent, ranging from 100 to 1000 nm; insights into their sub-cellular origin are usually obtained post-isolation by detecting the enrichment of specific markers [6]. For these reasons, the term small/large EVs can be also used to refer to a mixed population of vesicles with a defined range of size [7]. Recently, EVs have been studied in the frame of the modulation of the tumor microenvironment and inflammation [8]/immune surveillance [9], or also investigated as carriers of therapeutics [10]. The high abundance of circulating EVs and a biological composition reflecting the cell of origin [11] qualify them as attractive diagnostic tool [12]. This potential has been recently demonstrated from liquid biopsies by detecting cancer biomarkers with recognized clinical utility, for example in the case of circulating levels of *EGFR* in lung cancer [13] and breast cancer [14] patients or *EGFR* mutations in pulmonary adenocarcinoma patients [14,15]; in the case of *KRAS*^{G12D} and *TP53*^{R273H} mutations in patients with advanced or early-stage pancreatic cancer [16,17]; in the case of copy number variations that matched genes frequently altered in metastatic prostate cancer patients [18].

However, the application of EVs into the clinical practice is still limited by low-throughput, time-consuming isolation procedures and the sensitivity and specificity of the results are highly dependent on the methods used to enrich them. Given their nanoscale dimensions, many technical challenges have been addressed to isolate them with purity and reproducibility [19]. The methods more frequently employed include differential and/or density gradient ultracentrifugation, immunocapture, microfiltration/size exclusion, or precipitation with hydrophobic agents [20]. The differential ultracentrifugation (UC) is the most widely applied [21], as it concentrates the vesicles and allows for size-based sedimentation of EVs according to the *g*-force applied without interferences from chemical additives, especially in view of downstream applications. In this case, the yield and the purity of the obtained EVs [22] are influenced by different protocol settings and challenged by co-sedimentation of protein aggregates [19]. For these reasons, new antibody-based strategies or EV-targeting probes have

been developed to recognize and immobilize the vesicles for subsequently detecting specific biomarkers [23–25]. These methods offer excellent throughput for identifying co-expression of antigens that decorate EVs, which should be deeply investigated in terms of quantitative/spatial distribution as potentially influenced by the cell status [5].

Alternative rapid EV-isolation procedures proven to reduce protein contaminants, in comparison with ultracentrifugation, exploited the negative surface charge of EVs [26–28]. These approaches are based on the principle that, under physiological conditions (pH > 5), heterogeneous EVs display negative fluctuations of zeta potential (ZP), which is a physicochemical parameter that quantifies the surface charge of biological particles [29]. ZP is highly dependent on pH, salt concentrations, temperature, and on the specific biochemical composition of the particles themselves [30]. Technologies like dynamic light scattering (DLS) [31] and tunable resistive pulse sensing (TRPS) [32] have been used to monitor the ZP of heterogeneous EVs, that encompasses –40 to –7 mV in PBS at pH 7.4 [33]. These values ensure the presence of a net negative surface charge that has been exploited to capture EVs and subsequently release them by modulating the pH and the ionic strength in the elution buffer.

In this work we describe an alternative strategy, named nickel-based isolation (NBI), that exploits a matrix of beads properly functionalized with nickel cations to capture heterogeneous EVs and the possibility to efficiently reverse the binding using a synergy of chelating agents (EDTA and citric acid) in PBS buffer (pH 7.4). NBI allowed a rapid enrichment of dimensionally heterogeneous (polydisperse) EVs in solution preserving their integrity and stability.

We characterized the performances of NBI in comparison with the gold standard differential ultracentrifugation and assessed the presence of specific hematopoietic-endothelial antigens on the surface of plasma-isolated EVs to ensure the unbiased enrichment of heterogeneous EV lineages by NBI. Importantly, the possibility to directly use NBI-isolated EVs as individual particles in no-wash, immobilization-independent assays allowed us to implement the amplified luminescent proximity homogeneous assay (alpha) and a new droplet digital PCR (ddPCR) protocol to detect cancer-specific markers on EVs from the plasma of oncological patients with an unprecedented resolution from liquid biopsy.

2. Materials and methods

2.1. Cell cultures

Glioblastoma cells U87-MG (ATCC® HTB-14™); breast adenocarcinoma cell lines MCF7 (ICLC; HTL95021) and MDA-MB-231 (ICLC; HTL99004), neuroblastoma SH-SY5Y (ATCC® CRL-2266™), prostate adenocarcinoma PC-3 (ATCC® CRL-1435™), and melanoma SK-MEL-28 (ATCC® HTB-72™) cells were grown in DMEM, except for PC-3 cell line that was cultured in standard conditions in RPMI 1640 Medium, supplemented with 10% Fetal Bovine Serum, 2 mM L-glutamine, and 100 U/ml penicillin + 100 µg/ml streptomycin (all from Life Technologies, Carlsbad, CA, USA) to obtain complete medium. Generally, to obtain extracellular vesicles (EVs)-containing media, cells were initially grown in complete medium until reaching 75% confluence (usually 48 h); then, after two gentle washes with PBS, cells were incubated with serum-free medium for 24 h. Cells were plated in different plastic formats according to the experiments to be performed, but the density of them was kept constant at $3.2 \pm 0.2 \times 10^4/\text{cm}^2$ otherwise differently stated in the figure legends.

Before starting NBI procedure, collected media were centrifuged at 2800g for 10 min and carefully transferred to new tubes.

For the experiments in Fig. 2a, dFBS condition refers to NBI performed in media containing 100 K ultracentrifuged FBS at final concentration of 10%. These media have been diluted 1:10 with PBS to reduce viscosity of the solution.

For cell density experiments in Fig. 2B, U-87-MG, MDA-MB-231, SH-SY5Y, MCF7 and PC-3 cell lines were plated in triplicates in 6-well plates with these numbers per well: 3.4×10^5 ; 1.7×10^5 ; 8.5×10^4 ; 4.2×10^4 ; 2.1×10^4 and 1.0×10^4 . After 48 h of incubation in complete medium, cells were washed twice with PBS and then incubated for 24 h with serum-free medium before starting with NBI protocol. In this case, after removing EVs-containing media, adherent cells were fixed with 4% paraformaldehyde, stained with Hoechst33342 and washed with PBS for high content imaging analysis using Operetta instrument (Perkin Elmer). Images were acquired at 10 \times magnification and 50 fields/well were analysed by Harmony software. EVs were analysed by TRPS using qNano (IZON Science).

2.2. EVs isolation by differential ultracentrifugation

EVs produced by U87-MG cells grown in T150 flasks (CLS430823-50EA) were isolated by differential ultracentrifugation according to the protocol by Di Vizio et al. [34] with minor modifications. Briefly, after 24 h of incubation with cells serum-free media were collected in falcon tubes and centrifuged at 2800g for 10 min at 4 °C to mainly remove cell debris and apoptotic bodies. Then, the supernatants were transferred to ultracentrifuge tubes (Polyallomer Quick-Seal centrifuge tubes 25 \times 89 mm, Beckman Coulter) and centrifuged at 10,000g for 30 min at 4 °C in the Optima XE-90 (Beckman Coulter) instrument with SW 32 Ti rotor. This step allowed to preferentially precipitate larger particles (less apoptotic bodies, microvesicles), that were gently resuspended in filtered PBS (Res1). Thereafter, supernatants were further centrifuged at 100,000g for 70 min at 4 °C to pellet smaller particles. Pellets were resuspended in filtered PBS (Res2). The volumes of Res1 and Res2 were pooled and stored at -80 °C or kept at 4 °C to proceed with TRPS analyses. For experiments involving OptiPrep density gradient (ODG) preparations, we followed the protocol reported by Van Deun et al. [35], but starting from a volume of 200 μ l of PBS, that resuspended the pellet of 100,000 g ultracentrifuged particles, loaded on the top of 5–40% iodixanol gradient. After ultracentrifugation, we pooled the fractions 8 to 10 and analysed by immunoblotting the pellet obtained by re-centrifugation at 100,000g for 2 h from a 3 ml solution.

2.3. Flow cytometry analysis of microvesicles

Vesicles obtained by differential ultracentrifugation or NBI were diluted in 0.22 μ m filtered PBS and background signal was set up on filtered PBS and the light scattering threshold level was adjusted to allow an event rate of ≤ 5 events per second.

Light scattering detection was performed in log mode, the assigned voltages for FSC and SSC were 300 and 310 V, respectively, and the threshold was set at 200 for both signals. Acquisition was performed at low flow rate and samples were properly diluted to avoid coincidence and swarm effects. Bead standards of 1 and 10 μ m (Invitrogen) were used to set gates for microvesicles. A number of 10,000 events was counted or at least 1 min recording for each sample. Sample acquisition was performed on a FACS Canto flow-cytometer (BD Biosciences) and data analysis using BD Diva software (BD Biosciences).

2.4. Nickel-based isolation (NBI)

Positively charged agarose beads (GE Healthcare, 17-5268-01) were prepared with a suspension of 20 mg/ml in PBS containing 190 mM of NiSO₄ (Sigma, 656895). Residual amount of cations was removed by repeated PBS washing and centrifugation and beads were stored at 4 °C for up to 1 month.

The capture of EVs has been optimized using 20 μ l/ml of beads from the prepared suspension and entirely performed at room temperature. An excess of beads ensured better reproducibility and maximal EVs recovery. Briefly, beads were gently added on the upper surface of the EVs-containing medium and the solution placed in orbital shaking for

30 min, well homogenized during incubation. Thereafter, tubes were gently centrifuged (~ 200 g) and then maintained in vertical position for 5 min to allow beads to settle down by gravity. The elution buffer, freshly prepared by diluting solution A (3.2 mM EDTA, ThermoFisher, UltraPure pH 8.0, 15575020) and B (10 mM NaCl, Sigma, 450006, 45 μ M citric acid, Sigma, 251275) in 0.22 μ m-filtered PBS allowed competitive EVs-beads dissociation and release of EVs in solution at physiological pH (7.4).

2.5. Transmission electron microscopy (TEM)

The vesicles were visualized using conventional transmission EM (TEM). Briefly, a 5 μ l aliquot of a purified sample, fixed in elution buffer with 2.5% formaldehyde, was applied to 300-square mesh copper-nickel grids coated with a thin carbon film. The grids were subsequently negatively stained with 1% buffered uranyl acetate, pH 4.5, and observed using a TEM FEI Tecnai G2 Spirit microscope operating at 100 kV and equipped with an Olympus Morada side-mount 2K \times 4K charge-coupled device camera (magnification used: 20500 \times and 87,000 \times).

2.6. TRPS (tunable resistive pulse sensing)

Size and concentration of the EVs were characterized by TRPS using qNano (IZON Science). An average of 500 particles were counted for each sample, except for experiments performed in 6-well plates (Fig. 2B, Fig. 3, and Fig. S4) or in samples where the particle rate was below 100 particle/min, in which at least 2 min recording time was used. NP200 (A40948, A43545, A43667, A43667), NP400 (A43592, A44117, A44116), NP800 (A40542, A36164, A40548, A44118) and N1000 (A40572) nanopores, stretched between 45.5 and 47 mm were used. Voltage was set in between 0.12 and 0.68 to achieve and maintain a stable current in the range of 95–130 nA, noise below 7–12 pA and particle count rate linear. The calibration beads CPC100B (Batch ID: B8748N), CPC200B (Batch ID: B6481M), CPC500E (Batch ID: 659543B), CPC800E (Batch ID: 634561B) and CPC1000F (Batch ID: 669582B) with mean diameters of 114 nm, 210 nm, 500 nm, 710 nm and 940 nm, respectively, were from IZON Science. All the qNANO data were recorded and analysed by IZON Control Suite v.3.

2.7. Protein competitive assay

The step of EVs elution has been challenged by a competitive assay in which 10 ml of medium containing EVs deriving from U87 cells was supplemented with 30 μ g/ml of DH5 α *E. coli* crude extract and with 15 μ g/ml of purified histidine-tagged recombinant proteins (T7 RNA pol, 110 kDa; HuR, 36 kDa; YTH, 23 kDa). Briefly, DH5 α cells were grown in LB medium until they reached an OD₆₀₀ of 0.5 and were harvested by centrifugation at 6000g for 5 min. Pellet was resuspended in 3 ml of DMEM medium + 1 μ g/ml lysozyme and sonicated at 4 °C in water bath for 7 cycles (40 amplitude, 7 s on, 10 s off). Lysate was clarified by centrifugation at 13,000g for 20 min and then filtered with 0.2 μ m membrane disposals prior to be spiked to the EVs-containing medium. Histidine-tagged recombinant T7 RNA polymerase was kindly provided by Dr. S. Mansy's lab (CIBIO, University of Trento); recombinant HuR [36] and YTH [37] proteins produced and purified as previously described.

NBI was performed with incubation times and reagents already described, except for the gradient of elution solutions as indicated in Fig. 1b. Protein samples were quantified using BCA and Bradford assays according to the manufacturer's instructions. Equal volume of eluates were loaded on 12% SDS-PAGE for subsequent Sypro Ruby staining or western blotting using a 1:1000 dilution of a primary anti-histidine antibody (ab1187).

Number and size of recovered particles were analysed by TRPS, in all the fractions, using NP800, NP400, and NP200 nanopores.

For IP with apolipoproteins, 50 µg of whole cell lysate and the lysate of EVs isolated from the media of three T150 flasks per each condition: UC and NBI) were separated by a pre-cast gradient SDS-PAGE (Bolt™ 4–12% Bis-Tris Plus Gels, 12-well, Invitrogen) and transferred to a polyvinylidene difluoride membrane (Amersham Hybond P 0.2 µm PVDF) overnight. After blocking with 5% nonfat milk in TBS-T (10 mM Tris, pH 8.0, 150 mM NaCl, 0.1% Tween 20) for 60 min, the membrane was incubated in 1% milk TBS-T with antibodies against Apo B100 (ab7616, Abcam, 1:1000), Apo A1 (ab7613, Abcam, 1:1000), Syntenin (1:1000), Flotillin-1 (1:1000), Alix (1:1000) at 4 °C overnight. Membranes were washed three times for 5 min and incubated with horseradish peroxidase-conjugated anti-goat, anti-rabbit or anti-mouse

secondary antibodies for 1–2 h. Blots were washed with TBS-T three times and the immunoblot signal was revealed using the chemiluminescent ECL Select detection reagent (GE Healthcare Amersham, UK).

2.8. Preparation of exosome-like liposomes

The lipid composition of exosome-like vesicles was: 20% mol egg phosphatidylcholine, 10% mol egg phosphatidylethanolamine, 15% mol dioleoylphosphatidylserine, 15% mol egg sphingomyelin, 40% mol cholesterol (adapted from literature [38,39]). Lipid films were formed by removing the organic solvent (i.e. chloroform) from a lipid solution by rotary evaporation and vacuum drying for at least 1 h. Lipids at a

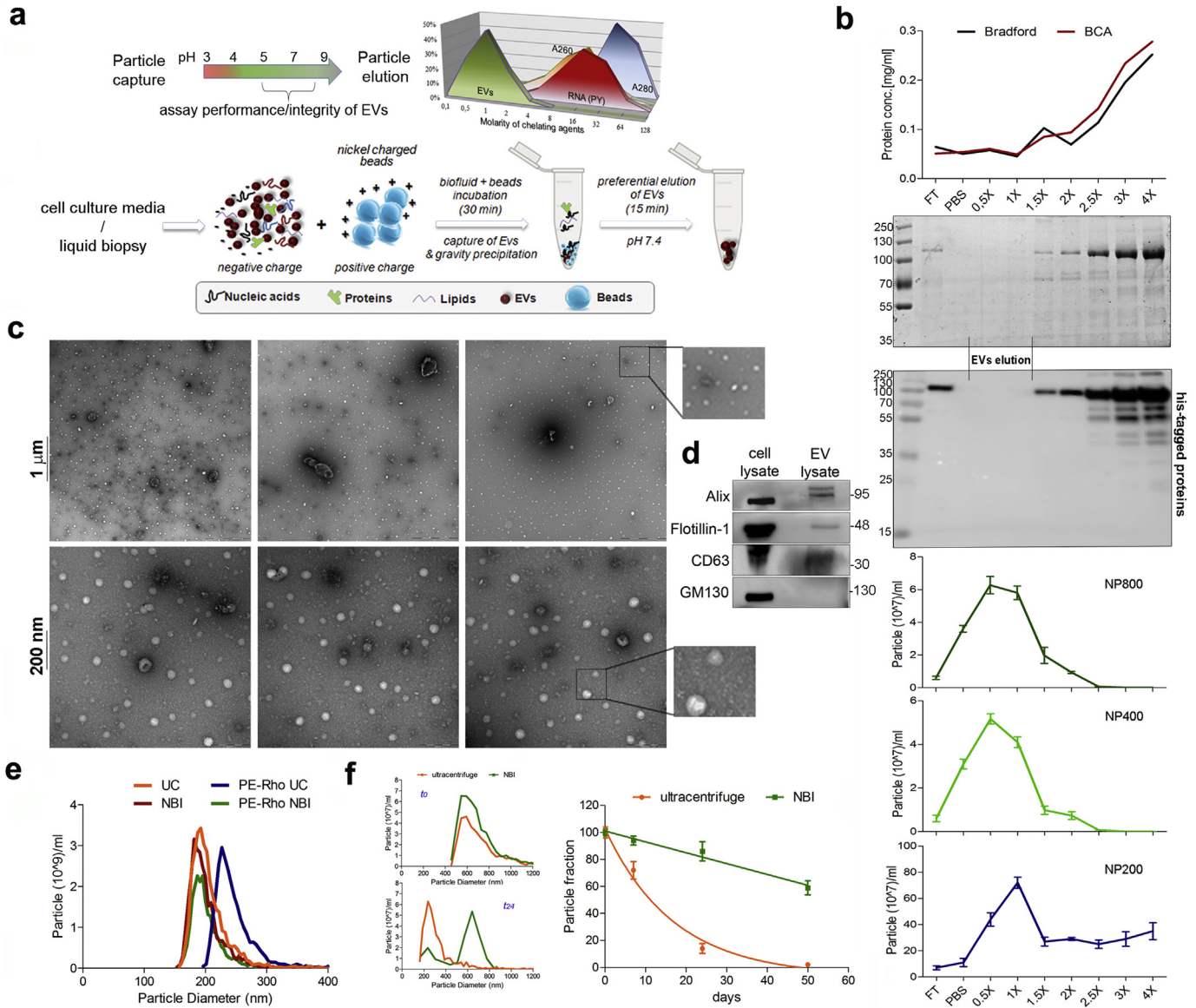


Fig. 1. Rapid purification of EVs by NBI preserving their integrity, dispersity, and stability in solution. a) At pH values >5 the net negative charge of membranous particles makes them susceptible to electrostatic interactions. Using 1–3 mM of chelating agents, TRPS analyses detected particles in the 500–700 nm range of size, selectively eluted from a functionalized stationary phase in contrast to nucleic acids (A260), proteins (A280), or pre-stained ssRNA (RNA Y) pre-incubated with nickel-agarose beads. The procedural steps highlighting the rapid NBI procedure are depicted. b) Competitive assay in serum-free medium containing 500 µg/ml of DH5α protein extract and of 50 µg/ml each of purified his-tagged proteins (T7p07, HuR, YTH domain). Two parallel gels were exposed to SYPRO Ruby or blotted on PVDF membrane to detect histidine (tag known to confer the strongest interaction with Ni). The 1× solution is the optimized buffer and the flow-through (FT) is the medium after beads sedimentation. qNANO analyses with indicated nanopores were performed and SD refers to two independent experiments. c) Transmission electron microscopy (TEM) acquisitions, with 3 fields at 20.500× (1 µm) + 5× magnification and 3 fields at 87.000× (200 nm) + 5× magnification, of NBI samples fixed with 2.5% paraformaldehyde in the elution buffer. The original scale bars are embedded at the bottom right, but also added manually on the left side for better visualization. d) Western blot analyses on EV lysate (recovered by 14 × 10⁶ cells) and on 1% total cell lysate (TCL) of U87 cells. e) Mixture of 4.2 × 10⁹ liposomes with a diameter of 181 ± 23.8 nm recovered by ultracentrifugation (UC) or NBI. The same experiment has been replicated with phosphatidylethanolamine-rhodamine (5 ng/ml) stain (PE-Rho) of liposomes prior UC or NBI processing. f) EVs were isolated by UC or NBI from 3 ml of serum-free medium of U87 cells and analysed at (t₀) or after 24 days (t₂₄, stored at 4 °C). Repeated measurements by TRPS have been performed until 52 days post-purification and the relative half-life of the 600 nm populations have been calculated with GraphPad Prism software v.5.

final concentration of 1 mg/mL, were swollen in DPBS and vortexed vigorously to give multilamellar liposomes, which were further exposed to 6 cycles of freezing and thawing. Exosome-like liposomes were prepared by extruding a suspension of multilamellar liposomes with a two-syringes extruder (LiposoFast Basic Unit, Avestin Inc.). Thirty-one passages were performed through two stacked polycarbonate filters (Millipore) with pores of different average diameters to obtain differently sized vesicles [40], then measured by photon correlation spectroscopy with a Zeta Sizer instrument (Nano-ZS, Malvern Instruments).

2.9. Blood samples

Plasma samples derived from patients with metastatic colon cancer were provided by the IRST Cancer Center. All patients gave informed consent before blood sampling, approved by the Local Ethics Committee. Patients' tumors were characterized for BRAF status by MassARRAY (Sequenom, San Diego, CA, USA) using the Myriapod Colon status (Diatech Pharmacogenetics, Jesi, Italy). Plasma was obtained from peripheral blood collected in EDTA-tubes, after centrifugation at 3000 rpm for 15 min, and stored at -80°C until EV isolation.

Whole blood from healthy donors were collected at Meyer Children's University Hospital. Plasma samples were collected into commercially available anticoagulant-treated tubes EDTA-treated (lavender tops), serum samples in red topped tubes. The venous blood in EDTA tube was shipped on cold packs from hospital blood collection unit to the laboratory. Informed consent were obtained from donors before the sample analysis.

Plasma has been obtained by removing cells after centrifugation for 10 min at 2000g using a refrigerated (4°C) centrifuge (Eppendorf 5702 R, Milan, Italy). Serum samples have been obtained allowing the blood to clot by leaving it undisturbed at room temperature for 30 min. The clot has been removed by spin down at 2000g using a refrigerated (4°C) centrifuge (Eppendorf 5702 R, Milan, Italy). Blood count were performed using a Sysmex XE-5000 hematology analyzer (Sysmex America, Mundelein, IL). The analytic procedure was conducted according to the manufacturer's instructions.

Blood from metastatic prostate cancer patients was obtained at Weill Cornell Medicine (WCM) after informed consent (IRB #1305013903). Whole blood (Streck Cell-Free DNA BCT) was centrifuged at $1600\text{ g} \times 10\text{ min}$ at 4°C within 3 h after blood collection. The plasma layer was transferred to 2 ml microcentrifuge tubes and centrifuged at $16,000\text{ g} \times 10\text{ min}$ at 4°C . The plasma was then collected and stored at -80°C . Complete blood counts (CBC) was performed in the WCM clinical lab and results obtained from chart review.

Immunodepletion of NBI-purified vesicles has been performed using biotinylated anti CD235a (130-100-271) and anti CD41a (130-105-608) from Miltenyl Biotec, anti-AL-CAM (sc-74558), anti-MEL-CAM (sc-18837), anti CD45 (sc-1187) from SantaCruz Biotechnology, and streptavidin (11205D) or protein-G (10003D) dynabeads from Thermo Fisher Scientific. Vesicles after beads precipitation have been measured by qNANO and normalized to the number of particles in the counterpart control samples with equivalent amount of biotin (Sigma, B4501).

2.10. Tumor sample analysis

Formalin fixed and paraffin included (FFPE) patients' tumor samples, used for routinary molecular diagnostic, were selected for containing an area of at least 50% of tumor cells, based on hematoxylin and eosin staining. Tumor genomic DNA was extracted with QIAamp DNA Micro kit (QIAGEN, Hilden, Germany), following the manufacturer's protocol, and DNA quantity and quality was determined at Nanodrop (CELBIO, Milan, Italy). Characterization of BRAF status was performed by Pyrosequencing with the anti-EGFR MoAb response® BRAF status assay (Diatech Pharmacogenetics, Jesi, Italy): 50 ng of starting FFPE genomic DNA were amplified and reactions were run on the PyroMark Q96 ID system (QIAGEN), according to Diatech Pharmacogenetics

protocol. For samples 7, 12, 13, 23, and 26, Qualitative detection of BRAF-V600E and KRAS-G12D/G12C mutations was repeated on 30 ng of tumor DNA, by using either the Easy®BRAF kit or the Easy®KRAS kit, on Corbett Rotor-Gene 6000 (QIAGEN), following manufacturer's instructions (Diatech Pharmacogenetics). The assay allows the detection of low percentages of mutated allele by real-time amplification with sequence-specific probes: positivity for BRAF-V600E was considered over the internal BRAF control, as a delta Ct lower than 12.5 cycles, and setting the detection threshold on 0.04, according to the guidelines of Diatech Pharmacogenetics.

2.11. RNA extraction

Total RNA was extracted using QIAzol reagent (QIAGEN) according to the manufacturer's instructions with several modifications. Briefly, 100 μl of QIAzol was added directly to the beads before the elution step of NBI, vortexed and incubated for 5 min at room temperature, supplemented with 20 μl of chloroform, shaken vigorously for 15 s and incubated at room temperature for 3 min. Phases were separated by centrifugation at 12,000g for 15 min at 4°C , and the upper phase was recovered. After addition of 1 μl of glycogen (20 mg/ml) and 100 μl of isopropanol, RNA was precipitated overnight at -80°C . After centrifugation at 12,000g for 10 min, RNA pellets were washed with 75% ethanol, centrifuged as above and resuspended in 10 μl RNase-free water. RNA was quantified using the Bioanalyzer RNA 6000 Pico Kit (Agilent Technologies) following the manufacturer's instructions.

2.12. Amplified luminescent proximity homogeneous assay (alpha)

Reactions were carried out in 384-Optiplate (Perkin Elmer) in a final volume of 20 μl . Assay was optimized in PBS using 15 $\mu\text{g}/\text{ml}$ of nickel-chelate AlphaLisa Acceptor beads and 10 $\mu\text{g}/\text{ml}$ of streptavidin-Donor beads with serial dilutions of antibody to identify hook point. The presence of surface markers was analysed in dose-response with serial dilution of EVs, previously characterized by TRPS. EVs were purified by NBI from plasma of healthy donors or from serum-free medium of tumor cell lines. Alpha counts were revealed by Enspire instrument (Perkin Elmer) after 90 min of plate incubation in the dark at room temperature. We used a biotinylated antibody against human PSMA (Cusabio, CSB-PA018865LD01HU) and a recombinant his-tagged PSMA (Origene, NM_002786) for a standard curve quantification.

2.13. Reverse transcription and droplet digital PCR

Reverse transcription was performed using miRCURY LNA Universal RT microRNA PCR, Universal cDNA Synthesis Kit II (Exiqon) following the manufacturer's instructions with the following reaction composition: 2.3 μl of 5 \times reaction buffer, 1.15 μl enzyme mix, 0.5 μl synthetic RNA spike-in and 7.5 μl of template total RNA.

QX200TM Droplet Digital™ PCR System (BioRad) was used to quantify mRNA copies using EvaGreen chemistry and the following primers: 5'-CAACGAATTTGGCTACAGCA-3' and 5'-AGGGTCTACATGGCAACTG-3' for *GAPDH*; 5'-GATTTTGGTCTAGCTACAGA and 5'-GGATT TTATCTTGCATTC for *BRAF*.

The direct encapsulation of EVs into oil droplets has been performed using isolated EVs as input sample, EvaGreen master mix supplemented with 5 U/ml of WarmStart® RTx Reverse Transcriptase (NEB) and with 3 mM magnesium sulphate. The standard protocol of ddPCR included a starting 10 min step at 55°C followed by 5 min at 65°C .

We optimized the procedure working with 10^2 – 10^6 polydisperse EVs to obtain at least 15,000 droplets in each assay.

2.14. Statistical analyses

The data and the number of independent experiments are indicated in the relative figure legends. Anova, *t*-test, and Pearson r coefficient

were calculated by GraphPad Prism Software v5.1, and results were considered statistically significant when P value was <0.05 (*), <0.01 (**), <0.001 (***)).

3. Results

3.1. Capture and competitive elution of extracellular vesicles by nickel-based isolation

The versatility of NBI is based on the scalable range of positive charge conferred by nickel cations and on the surface area of a stationary phase. We used a suspension of agarose beads functionalized by increasing concentrations of nickel sulphate (50–300 mM). To have an indication on the number of particles recovered from the beads, we analysed the particles obtained from 10 ml of serum-free media incubated with U87 glioma cells in parallel with differential ultracentrifugation (UC). As estimated by flow-cytometry and only for events ≥ 0.5 μm , we reached a condition where the observed number of particles was equivalent for the two approaches and, in case of NBI, dependent on nickel cations, since no particles were recovered by non-functionalized beads (Fig. S1). These results have been obtained by functionalizing a suspension 20 ml/ml of beads, 24 ± 7 μm in size, with 200 mM of nickel sulphate.

Since different molecules can efficiently interact with a nickel matrix, we next used TRPS (qNANO instrument) [41] and spectroscopic analyses to analyse the number of particles eluted from the beads in the presence of a phosphate buffered saline (PBS) solution containing chelating agents (elution buffers), i.e. EDTA and citric acid (CA), trying to design an elution buffer tailored for EVs. We used 10 ml of media containing U87-derived secretome and, in control experiments, we used nickel-beads pre-incubated with U87-purified input DNA, input proteins, or input RNA, to understand the specificity of the elution buffer in the reversible binding of the different biomolecules. We monitored, by absorbance and fluorescence scan, both elution buffers and beads (in this case by further normalizing the signal to the 350 nm peak of nickel beads). Since the absorbance of DNA and RNA molecules has the same peak at 260 nm, we pre-stained the beads with pyronin Y in order to measure a specific fluorescence signal for the RNA. We detected a significant number of particles ($2\text{--}5 \times 10^9/\text{ml}$, 50–700 nm using 3 nanopores) with the elution buffer containing a low millimolar range of chelating agents (molar ratio EDTA:CA of $\sim 1:70$; elution buffer 1 \times), which resulted to an early dissociation of qNANO detected particles (K_d of 1.15 ± 0.37 mM^{-1} for EDTA in the presence of 45 μM of CA) at pH 7.4. Notably, no absorbance or relevant fluorescence signals were obtained using the elution buffer 1 \times , in contrast of elution buffers containing >3 mM of EDTA. Representative data and the steps of the procedure are schematically shown in Fig. 1a.

To validate these observations with complementary approaches, we challenged this selectivity by competitive assays in a protein-enriched system. We supplemented 10 ml of DMEM, containing the secretome of U87 cells, with crude extracts of DH5 α *E. coli* cells (from pelleted bacteria) and with 3 purified histidine-tagged proteins of different molecular weight (MW, Fig. S2), since nickel matrices are conventionally exploited to purify 6xHis recombinant proteins. We performed NBI in the mixture and eluted the particles with a gradient of chelating agents in PBS, keeping the reference of the elution buffer 1 \times solution. Captured proteins started to be detected/eluted with a 1.5 \times solution, as evidenced by SDS-PAGE, SYPRO Ruby staining and immunoblotting using an anti-his antibody, that firstly detected the recombinant proteins with higher MW (Fig. 1b). In the same samples, TRPS analyses with 3 nanopores detected 50–700 nm particles with 0.5 \times and 1 \times elution buffers, confirming the competitive dissociation of EVs from the beads in the low millimolar range of chelating agents. According to Bradford or BCA assays, we quantified 20–25 $\mu\text{g}/\text{ml}$ (0.5 \times + 1 \times condition, Fig. 1b) of proteins that mirrored a total of 2×10^9 particles detected by the nanopores.

The strategy of using EDTA combined with citric acid provided a valuable alternative to preserve the pH and the biological sample from high concentrations of salts [27] that can affect vesicles' integrity, as shown in Fig. S3.

We evaluated the extent of particles obtained with elution buffer 1 \times by transmission electron microscopy (TEM; 20,500 \times and 87,000 \times magnifications, Fig. 1c). Wide-field acquisitions of NBI samples showed a broad dispersity of vesicles with an enrichment at 80–120 nm in size. Although we optimized these experiments with reduced concentration of formaldehyde and dry time to minimize the shrinkage effects [5], we used DLS to calculate the polydispersity (index of 0.61 ± 0.05), which mirrored the data obtained by TRPS. Western blot analyses on those samples showed that NBI-isolated EVs were positive to endosome-associated proteins, such as Alix and CD63 markers [42], or also found to the plasma cell membrane, such as Flotillin-1 [43], and negative to Golgi markers (GM130, Fig. 1d) [20], at least indicating the presence of exosome and microvesicle markers in the mixed populations of the vesicles we isolate.

With the aim to investigate the impact of mechanical forces exerted during the NBI procedure, we produced liposomes with an “exosome-like” lipidic composition [39] and spiked them in 10 ml of DMEM (Fig. 1e). Similar to the EVs in the same conditions, the average zeta potential of these preparations was -15.2 mV, as determined by DLS. Testing a small volume (0.5 ml) of media, both NBI and UC allowed near full recovery (98.6%) of input liposomes with a mean size of ~ 190 nm, although with a slight shift of ~ 10 nm of diameter in UC samples (orange vs red curve). Additional experiments performed with liposomes that we pre-stained with the lipophilic phosphatidylethanolamine-rhodamine (PE-Rho) dye evidenced a coalescent effect (>40 nm shift) of PE-Rho UC vesicles, not observed with PE-Rho NBI vesicles. These data demonstrate that the elution buffer used for NBI minimizes particles aggregation. We next interrogated the turnover of vesicles stored at 4 $^\circ\text{C}$ after purification by NBI or UC (Fig. 1f, left). We focused on particles ≥ 300 nm, more vulnerable than smaller vesicles to different storage conditions [44]. In UC samples, at 24 days post-isolation (t_{24}), the 600 nm population originally present was virtually replaced by a population of ~ 300 nm. Strikingly, NBI samples retained the 86% of the original EV population, still detectable using the same nanopore (Fig. 1f, middle). A kinetic analysis evaluating the size-shift of the 600 nm test population revealed a half-life of >50 days for NBI EVs, in contrast to 7.35 days for UC EVs (Fig. 1f, right). Collectively, these data indicate that polydisperse EVs can be selectively enriched by NBI preserving their integrity and stability in a near physiological pH solution.

3.2. Scalable and reproducible isolation of polydisperse EVs from cancer cell lines and the plasma of healthy volunteers

To assess the robustness of NBI in cell-based systems, we purified EVs secreted by U87 cells seeded at different densities, in 6-well plates, as indicated in Fig. 2a. We processed 1 ml of media and analysed the distribution of purified particles by TRPS using NP400, NP200, and NP100 nanopores. Isolated EVs displayed a continuous distribution, from approximately 50 to 700 nm in diameter (as compared with 3 different sets of iZON recommended calibration beads), characterized by at least two peaks of enriched vesicle populations showing ~ 200 and ~ 600 nm of mean diameter, respectively. We referred these two EV populations to as small EVs (sEVs) and large EVs (lEVs), respectively, while being aware of the unknown sub-cellular origin of individual NBI-isolated EVs [5]. The global number of isolated vesicles was proportional to the number of seeded cells, with a global coefficient of variation (CV) of 6.14% ($n = 9$ for NBI 1, 2, and 3) for both sEVs (197 ± 26 nm) and lEVs (595 ± 37 nm), underlying the high reproducibility of NBI. We did not observe a statistically significant variation ($P = .459$) comparing EVs from EV-depleted serum (dFBS) [45] and serum-free media (NBI 1), indicating that a reliable EV isolation can be started from relatively viscous solutions upon dilution with PBS. Interestingly, the efficient isolation of

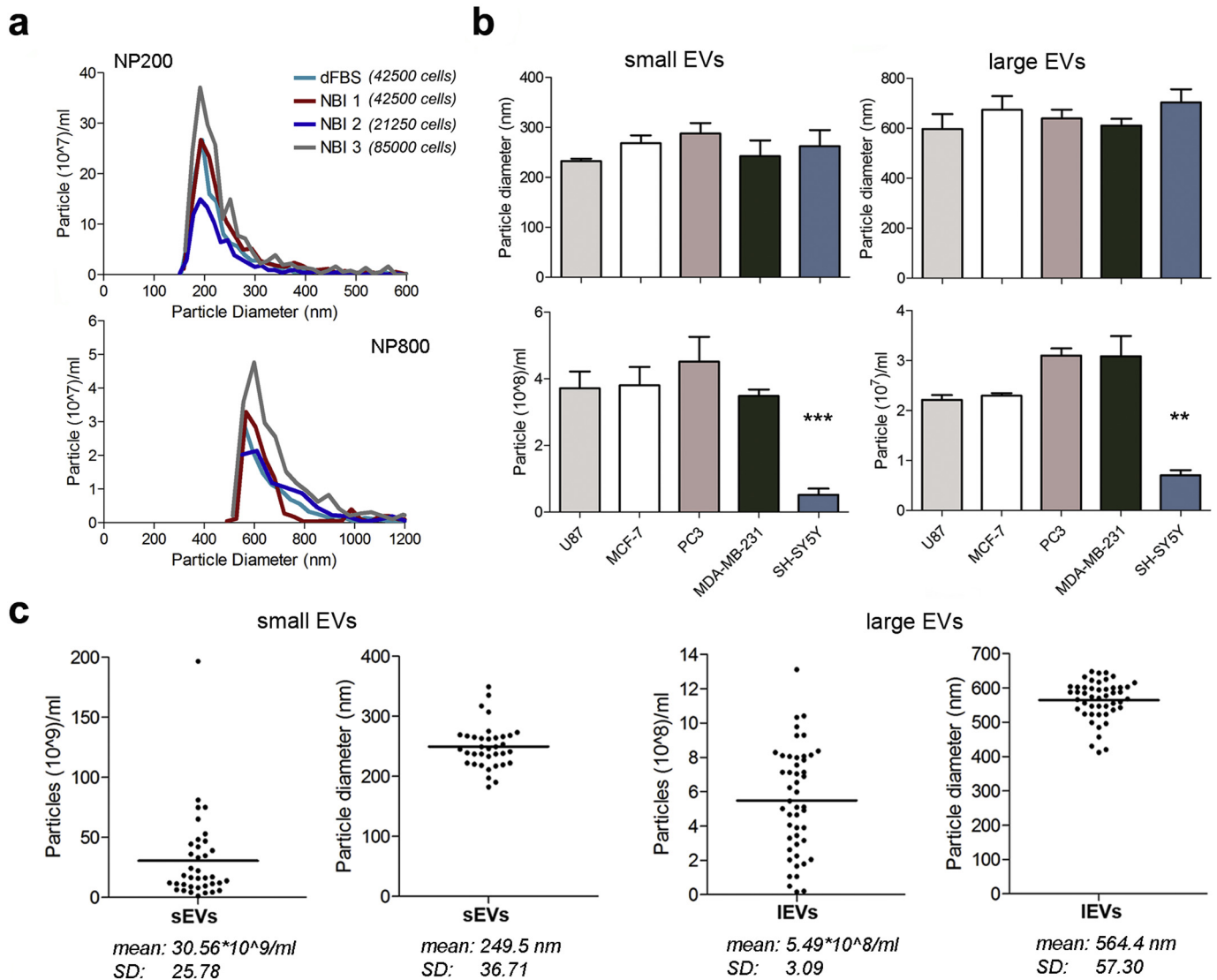


Fig. 2. NBI efficiently isolates EVs with high reproducibility from different biological fluids. a) The reproducibility of NBI has been tested in serum-free media of U87 cells seeded at different density, in 6-well plates, as indicated (NBI 1, 2, and 3). Ten % ultracentrifuged FBS (dFBS) condition showed substantial overlap with NBI-1 results. Plots are representative of 3 independent experiments and global CV was 6.1%. b) Distribution of NBI-isolated EVs have been analysed for different cell lines, as indicated. SH-SY5Y cells showed substantial reduction in releasing both vesicle populations (**P value = .006, $F = 70.13$, and *** < 0.0001 , $F = 30.84$, using one-way ANOVA and Bonferroni's post-test). SD refers to 3 independent experiments. c) NBI was applied to 0.5 ml of plasma obtained from healthy volunteers. The relative distribution of EVs (representative original profiles are shown in Fig. S5b) has been evaluated by TRPS analyses using 3 nanopores with the obtained concentrations, per milliliter of plasma, of the small and large EV populations.

EVs from small volumes allowed us to follow the release of vesicles using as low as 10^3 cells/cm² (Fig. S3). We observed a linear release of sEVs as a function of cell density, and an faster release of IEVs, as already suggested for microvesicles [5], possibly related with different biogenetic mechanism, intrinsic stability and/or cell-mediated turnover that correlate with particle size or composition [46]

We next characterized the EVs recovered from MCF-7, PC3, MDA-MB-231, and SH-SY5Y tumor cell lines (Fig. 2b). We observed an equivalent distribution of isolated EVs in terms of size and concentration, with the exception of the SH-SY5Y cells that demonstrated lower propensity to release both vesicle populations.

Since EVs are secreted in the blood by many cell types [47], we applied NBI to isolate EVs from the blood of healthy volunteers (Fig. S4). We analysed the abundance of isolated EVs in plasma and in the serum ($n = 9$) and clearly observed a 6-fold enrichment of EVs purified from plasma (Fig. S5a). We therefore performed NBI on (0.5 ml) plasma of 46 donors to assess the general distribution of EVs isolated from healthy subjects. The mean age of the volunteers was 45 ± 10 years. The profile of NBI-isolated EVs (Fig. S5b) was characterized by at least

two enriched populations showing a quantitative ratio of ~55:1: the first one with a mean diameter of 249.5 ± 36.71 nm (sEVs) and a concentration of $30.56 \pm 25.78 \times 10^9$ per milliliter of plasma; the second one with a mean size of 564.4 ± 57.3 nm (IEVs) and a concentration of $5.49 \pm 3.09 \times 10^8$ per milliliter of plasma, as indicated in Fig. 2c.

3.3. Characterization of plasma EV lineages by combined immunocapture

In line with other reports [48,49], mixed populations of circulating vesicles in healthy individuals are positive to hematopoietic or endothelial cell markers. We therefore investigated whether specific hematopoietic surface markers can be instrumental for the characterization of isolated EVs. We measured the number of plasma-isolated EVs left in solution after incubation with CD235a (marker of erythrocytes [50]) or CD41a (marker of platelets [51]) antibodies, i.e. immunodepleted samples. We observed a reduction of about 20% of the original population of microvesicles and of about 60% of sEVs using the CD235a. On the other hand, this trend was opposite using the CD41a, which showed preferential recognition of IEVs (Fig. 3a). These results indicate that plasma

isolated EVs expose markers that are specific of distinct cell lineages, underlying the derivation from different cells/progenitors. In addition, these results are in line with other reports indicating that platelet-derived microvesicles (range of size >300 nm) are abundant in the blood of healthy individuals [52,53].

With the aim to recognize specific EV lineages from a mixture of NBI-isolated polydisperse vesicles, we performed combined immunocapture experiments with a known amount of tumor-derived EVs spiked in the human plasma. We added 10^9 /ml EVs isolated from plasma to 10^9 /ml EVs isolated from the media of melanoma SK-MEL-28 cells. After NBI, we incubated the mixture of isolated vesicles with CD235a, CD41a, and CD45 antibodies (known to be expressed from leukocytes [54] but not from SK-MEL-28 cells [55]). After the immunoprecipitation (or immunodepletion) of CD235a, CD41a, and CD45 vesicles, the MEL-CAM antibody (CD146, expressed on the surface of SK-MEL-28 cells) still recognized the 64% of input EVs (light green vs light grey bars) positive to the epithelial marker, in contrast to the AL-CAM (CD166) antibody which resulted as an experimental negative control (Fig. 3b).

Therefore, specific hematopoietic markers could be instrumental to fractionate plasma NBI-isolated EVs into distinct EV lineages.

Importantly, the results obtained by these experiments indicated that intact, polydisperse EVs obtained by NBI form a homogeneous suspension of individual particles that could be exploited in no-wash, immobilization-independent assays.

3.4. Ultrasensitive detection of surface antigens on plasma EV lineages from healthy subjects and prostate cancer patients by NBI-alpha assay

Given their abundance in the blood, EVs can offer immediate advantage in liquid biopsy analyses for biomarker detection [56]. By NBI we can recover polydisperse EVs from biological samples and obtain a suspension of individual particles in solution. We therefore verified the possibility of applying NBI-extracted EVs to versatile homogeneous assays to perform ultrasensitive biomarker detection.

We adapted the amplified luminescent proximity homogeneous assay (alpha) [57] technology to detect surface antigens on NBI-isolated EVs. Following the notions obtained on the dispersity of NBI-isolated EVs, we designed the alpha assay using nickel-charged Acceptor beads in combination with streptavidin-Donor beads recognizing the antigen of interest through biotinylated antibodies (NBI-alpha,

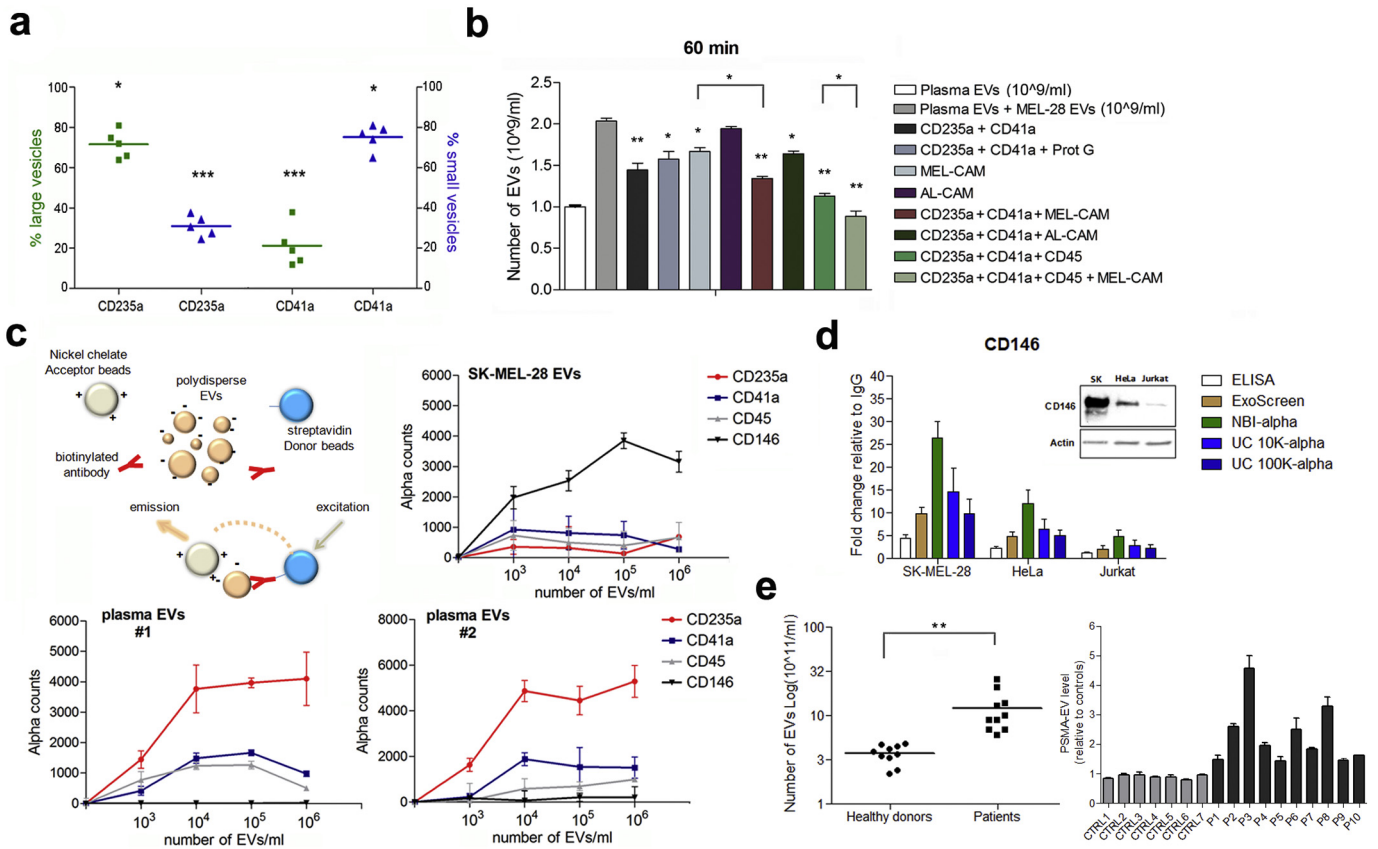


Fig. 3. NBI unbiasedly isolates different EV lineages from blood and allows to use EVs as individual particles in homogeneous assays to detect surface antigens. a) Hematopoietic cells' antigens, biotinylated anti-CD41a and CD235a antibodies, were used to characterize plasma isolated EVs. Isolated EVs (2×10^5 /ml), for a total of 15 samples, were divided in 2 volumes and incubated with biotinylated antibodies (CD41a or CD235a) + streptavidin dynabeads. Supernatants were analysed by qNano instrument and the distribution of EVs left in solution are shown. * *P* value < .05; ****P* value < .001. b) 10^9 /ml plasma EVs, together with 10^9 /ml EVs isolated from media of SK-MEL-28 cells were spiked in 1 ml of post-NBI human plasma. Indicated biotinylated antibodies were incubated for 60 min and, after streptavidin-dynabeads precipitation, TRPS analyses were performed on EVs left in solution. One-way ANOVA-Bonferroni have been used to calculate the statistical significance (**P* value < .05; ***P* value < .001). c) Diagram describing the alpha assay designed to detect surface antigens on individual, polydisperse EVs. Streptavidin-coated Donor beads recognize the antigen-specific biotinylated antibody; positively-charged nickel-chelate Acceptor beads interact with EVs and emit a fluorescent signal when in proximity of excited Donor beads. Saturation curves were obtained as function of number of EVs purified by NBI from plasma of two healthy donors (#1, #2) and from SK-MEL-28 melanoma cells. d) Cells lines expressing high, intermediate, or low levels of CD146 protein are indicated by immunoblotting performed on cell lysates. EVs were isolated by NBI or UC from the corresponding media of the three cell lines. The relative performances of different detection methods have been then evaluated, using anti-CD81 biotinylated antibody for plate-coating in the case of ELISA (coupled with anti-CD146 and HRP-conjugated secondary antibodies) or conjugation with Acceptor beads in the case of ExoScreen. The specific, background-subtracted signals were normalized to IgG signals of individual experiments. EVs for ELISA and ExoScreen have been isolated by UC. 10 K and 100 K indicate the *g* forces applied in the two protocols of UC, respectively. SD refers to two independent experiments. e) NBI was performed on 1 ml of plasma deriving from patients with advanced prostate cancer. Left: The relative number of EVs is plotted for healthy donors (50–55 years) and for prostate cancer patients (>60 years). One-way ANOVA-Bonferroni have been used to calculate the statistical significance. Right: the relative levels of PSMA on 10^5 EVs were detected by NBI-alpha. According to the standard curve with purified recombinant histidine-PSMA, 1 in the Y axis corresponds to ~35 pg/ml of PSMA in solution. SD refers to 3 independent experiments.

Fig. 3c). In these settings, we titrated the number of plasma-isolated EVs (#1 and #2) and of SK-MEL-28-isolated EVs as function of the signal obtained with biotinylated CD235a, CD41a, and CD45 antibodies. In the case of plasma EVs, the saturation curves obtained showed three to four times enhanced binding of CD235a with respect to CD41a and CD45, with a background signal for the epithelial marker CD146 even using 10^6 EVs (Fig. 3c, bottom left and right). Consistently with results in Fig. 2c,d, the CD235a antibody was the most efficient in recognizing a significant fraction of plasma-isolated EVs. In the case of EVs released from SK-MEL-28 cells, the signal of the CD146 antibody showed a dose-response curve, in contrast to the CD235a, CD45, and CD41a antibodies (Fig. 3c, top right), confirming the exposure of the CD146 protein on the EVs deriving from melanoma cells. All these experiments were performed in 20 μ l, using ~2% of the solution containing plasma EVs and ~20% of the solution containing EVs recovered from 3×10^5 SK-MEL-28 cells.

To challenge this approach in terms of sensitivity and accuracy, we used three cell lines expressing high (SK-MEL-28), intermediate (HeLa), or low (Jurkat) levels of the CD146 protein (see immunoblot in Fig. 3d). We isolated EVs using NBI or UC and evaluated 2 additional techniques (ELISA [58], ExoScreen [57]) for CD146 detection on EVs. Globally, all the results obtained were consistent with relative expression levels of endogenous CD146. The NBI-alpha demonstrated a higher dynamic range and the most performant detection (>5 times) of CD146 on EVs isolated from the most challenging Jurkat cells (FC = 4.6, Fig. 3d). By comparing the alpha assay results with samples enriched in large EVs (sedimented at 10,000 g) or in small EVs (sedimented at 100,000 g), respectively obtained by UC [59], we attributed the advantage of NBI-alpha in detecting the antigens on less aggregated particles (Fig. 1e).

We validated the NBI-alpha approach by detecting the prostate cancer specific membrane antigen (PSMA) on EVs isolated from plasma of prostate cancer patients (Fig. 3e). First, we analysed the distribution of EVs isolated from plasma of healthy subjects (age of 50–55 years) and from plasma of ten patients (>60 years) with metastatic prostate cancer (Fig. 3e). In line with other reports [60,61], we found a statistically significant increase (of about one order of magnitude) in the number of recovered EVs in the cancer patients (Fig. 3e, left). The Pearson r value of the correlation with counts of RBCs/WBCs/PLTs was 0.88 (Table S2). Using 10^5 EVs in the NBI-alpha assay, we detected higher levels of PSMA (mean P value < .001) in patients' EVs with respect to the healthy controls, reaching the sensitivity of picomolar concentration of PSMA (Fig. 3e, right) as determined by standard curve with his-tagged PSMA. Therefore, we specifically detected the enrichment of this surface marker on a fraction of the EVs isolated from the plasma of prostate cancer patients.

3.5. Ultrasensitive detection of RNA enclosed in EV lineages from plasma of healthy subjects and colon cancer patients by NBI-ddPCR assay

EVs can selectively or stochastically entrap nucleic acids [5]. The growing interest in exploiting EVs for cancer diagnostics relies with the potential identification of new biomarkers and of clues mirroring the genetic heterogeneity of tumor cells. Therefore, the potential clinical application requires a sensitive approach to distinguish EV sub-populations and to infer, at least qualitatively, the diversity of tumor cells that have originated them. We analysed the nucleic acid content of polydisperse EVs (50–700 nm) isolated from the plasma of healthy donors ($n = 47$) and we detected RNA, as demonstrated by automated electrophoresis profile following RNase treatment (Fig. S7a). One of the most highly sensitive reported technology to detect fractions of mutated transcripts enclosed within EVs is the droplet digital PCR (ddPCR) [17,62]. We therefore applied a standard ddPCR protocol to calculate the absolute number of *GAPDH* mRNAs in all the samples starting from $\sim 3 \times 10^9$ EVs (Fig. 4a and Fig. S7b). The system was sensitive enough to correlate the number of mRNA copies with the relative

counts of PLTs (Pearson r : 0.623; Fig. 4b), blood components already recognized as major producer of *GAPDH* [63]. Interestingly, given the quality of the EV samples obtained by NBI (in terms of non-coalescent particles), we had a chance to implement the ddPCR assay by directly encapsulating NBI-isolated EVs into the oil droplets, with a reaction mix containing a thermostable reverse transcriptase to perform a one-step amplification of the RNA fragment of interest (Fig. 4c). In these experimental conditions, specific nucleic acids can be rapidly detected from a discrete number of individual EVs and without the step of RNA extraction. Notably, particles isolated by UC failed to generate the expected number of oil droplets (>12,000), indicating that a direct encapsulation can be in this case hampered by aggregated vesicles.

We challenged the diagnostic performances of this NBI-ddPCR protocol by a retrospective analysis of a cohort of metastatic colon cancer patients. Patients were previously enrolled in a randomized phase III clinical trial for chemotherapy alone or in combination with bevacizumab [64,65]. All of the patients were analysed for the *KRAS* and *BRAF* status, two biomarkers that have a profound impact for patients in terms of clinical management and therapeutic options for CRC patients. We isolated EVs by NBI from the plasma of 21 cases with 6 additional blood draws collected from one single patient during the treatment (longitudinal liquid biopsy). The molecular characterization was performed by pyrosequencing on formalin-fixed, paraffin-embedded (FFPE) tissue DNA and indicated the presence of the *BRAF* V600E mutation in 5 out of 21 patients (~24%, samples C02, C11, C14, C20, and C25). The mutation was confirmed in the sample C03, a 5 months' later blood draw of the sample C20. In the samples we received, no mutations in *KRAS* were reported, except for the variant K117N in the sample C07. We analysed the samples in blind as in the order reported in Table S3.

First, we report that the levels of EVs recovered from plasma of colon cancer patients were strikingly higher in comparison to those of healthy donors (Fig. 4d). The correlation coefficient was 0.93 with relative counts of RBCs, WBCs, and PLTs. We then applied our RNA-extraction free ddPCR protocol in a reaction volume of 20 μ l and 10^3 isolated EVs as input to amplify the allele fragment containing the *BRAF* V600E mutation. As shown in Fig. 4e, the dots above an arbitrary threshold >1 indicate a relative higher number of mRNA copies detected by NBI-ddPCR, resulting from single droplets that have encapsulated vesicles carrying the V600E mutated transcripts. Indeed, samples C02, C03, C11, C14, C20, and C25 (orange dots) showed 100% matching with data obtained by pyrosequencing on FFPE tissues, while the samples C04, C09, C19, C21, and C24 (blue dots) indicated potential new insights on *BRAF* status only detected by NBI-ddPCR. To challenge the specificity and sensitivity of these results, we evaluated the extent of mRNA amplification upon immunodepletion of CD235a/CD41a positive EVs (Fig. 4e, middle). Unexpectedly, the number of *BRAF* V600E copies in the same patients' samples were found 4 to 5 fold increased with respect to the signal obtained from the bulk population of EVs, specifically increasing the dynamic range of sensitivity of the NBI-ddPCR. We also performed another experiment to analyse EVs isolated by anti-CD147, one of the most well-recognized approaches to enrich for colon cancer derived EVs [57] [66]. In this case, the diagnostic power was reduced to 83% as compared with the tissue biopsy results, with a number of copies <<1 in the case of the sample C25 (0.25 vs 4.48 and 20.05 copies, respectively obtained in the previous experiments), and to ~34% the concordance with blue dots. These data show that a significant fraction of EVs negative for the CD147 antigen can effectively carry *BRAF* mutated transcripts. Consequently, NBI is more efficient in comparison to single antibody-mediated enrichment of tumor-derived vesicles.

In order to validate the accuracy of the NBI-ddPCR results, we performed further inspections to the FFPE DNA of the samples from patients C04, C09, C19, C21, and C24, which resulted *BRAF* mutation positive in the EVs but not in the original tumor. These DNAs were subjected to a more sensitive, and clinically approved, allele-specific real-time PCR (EasyPCR) screen. The sample C19, that showed a value of

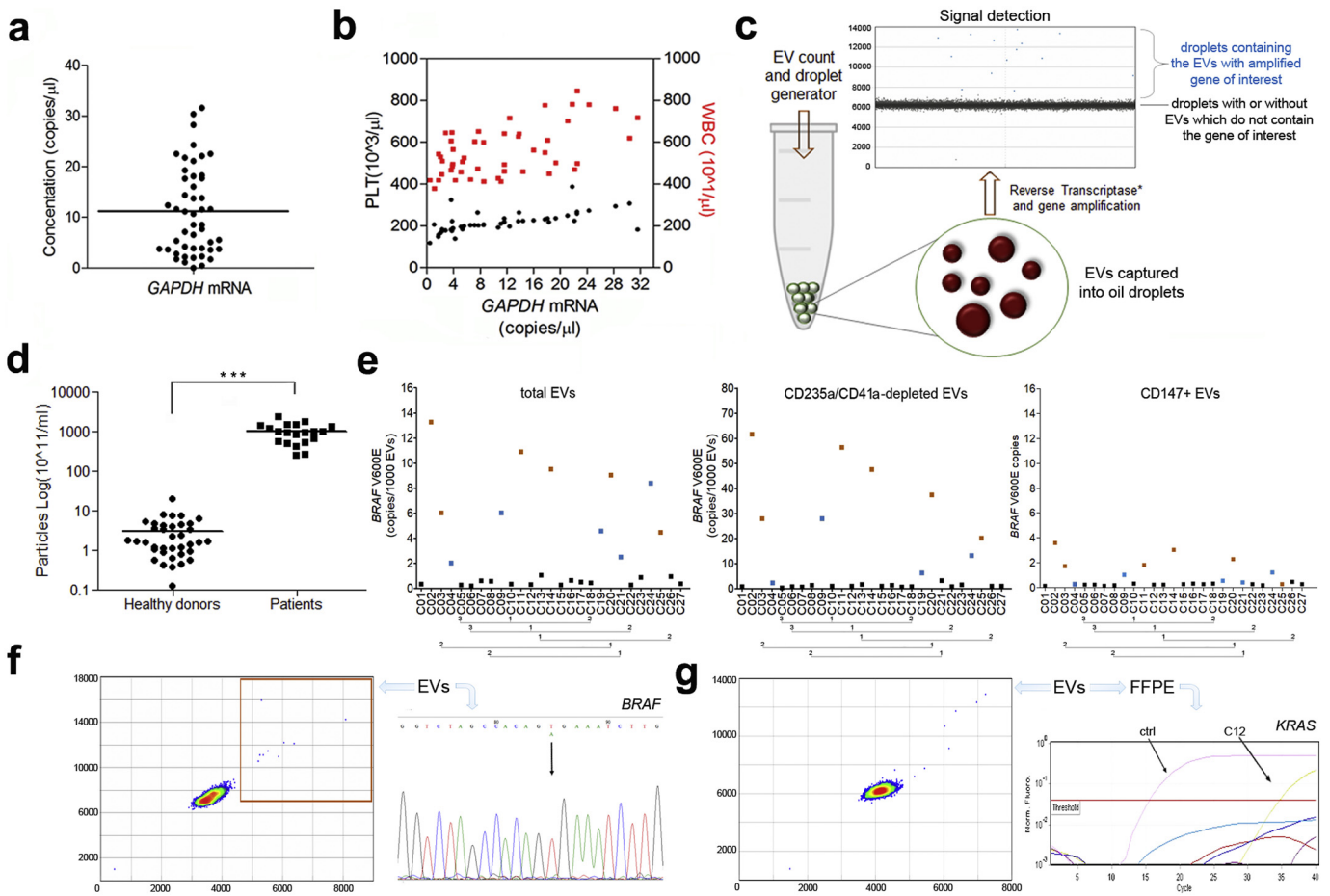


Fig. 4. Detection of RNA species enclosed into plasma-isolated EVs and design of a new ddPCR assay to exploit individual, polydisperse EVs for nucleic acids detection. a) Two μ l out of 20 of cDNA synthesized from 0.1–4 ng RNA. EV-RNA were deriving from plasma samples of 47 healthy donors. ddPCR has been performed with EvaGreen chemistry. Absolute number of *GAPDH* mRNA copies has been analysed by QuantaSoft Analysis software (BIORAD). b) The number of *GAPDH* mRNA copies positively correlated with number of PLTs ($r = 0.62$), major producer of circulating *GAPDH* mRNA and of microvesicles. c) Design of a new ddPCR assay to encapsulate EVs (50–700 nm) into oil droplets (1400–1600 nm). The number of copies of specific RNAs present in NBI-isolated EVs can be obtained as function of EV titration. The stochastic entrapment of EVs into oil droplets allow the amplification of the target of interest upon supplementation of the EvaGreen mix with a *thermostable Reverse Transcriptase enzyme. d) NBI was performed on 1 ml of plasma deriving from patients with colon cancer. The relative number of EVs is plotted for healthy donors (35–55 years) and for colon cancer patients (64 ± 8 years). One-way ANOVA-Bonferroni have been used to calculate the statistical significance. e) Left: the copy number of *BRAF* V600E enclosed in 1000 EVs isolated from 20 colon cancer patients is shown; middle: the copy number of *BRAF* V600E enclosed in 1000 EVs upon immunodepletion CD235a/CD41a positive EVs is shown; right: the copy number of *BRAF* V600E in EVs isolated by CD147 antibody. See the Table S3 to evaluate the matching with *BRAF* sequencing results performed in tissue biopsy. Numbered lines refer to longitudinal liquid biopsies from the same patient. f) Original plot of the NBI-ddPCR results for the sample C09, whose RNA from the bulk of EVs has been amplified with *BRAF* exon-spanning primers and then sequenced. g) Original plot of the NBI-ddPCR results for the sample C12 showing *KRAS* G12C mutation, subsequently verified by EasyPCR kit.

4.57 *BRAF* copies by NBI-ddPCR, resulted indeed positive to *BRAF* V600E mutation, indicating correspondence of the mutation at DNA level and the effective presence of this cell sub-populations in the tumor. In the efforts to highlight the presence of the mutated allele by standard sequencing in the sample C09, that showed a value of ~6 in the bulk EVs, we obtained a borderline A peak masked by the prevalence of the T allele present in the majority of the isolated EV (Fig. 4f). Therefore, by NBI-ddPCR we identified a previously unreported mutation in *BRAF* in at least the 7.5% of the colon cancer patients analysed. Notably, to investigate also the possibility of detecting a non-vesicular RNA proportion potentially bound by apolipoproteins that could be present in NBI-isolated samples, we performed immunoprecipitation with APO A1 and APO B100 antibodies on NBI-isolated EVs from the plasma of two healthy volunteers [67]. Fig. S7c shows that RNA extracted from particles recognized by APO A1 and APO B100 antibodies does not contribute to the signal observed for *GAPDH* or wild-type *BRAF* mRNAs.

Next, we succeeded to assess on the EVs from the same patients the prevalent mutations at the level of the exon 2 of *KRAS*. Remarkably, 3 samples resulted positive to the G12C mutation and 1 sample to the G12D: the presence of the G12D allele in the sample C12 (with a value of 1.79 copies/ 10^4 EVs) was clearly confirmed by a re-analysis on FFPE

DNA (Fig. 4g). Even in the case of *KRAS*, by NBI-ddPCR we revealed a previously undetected mutation for at least 3.8% of the patients analysed.

Collectively, these data show that NBI-ddPCR can be used for liquid biopsy analyses and to detect clinically relevant predictive and prognostic biomarkers (such as *KRAS* and *BRAF*) and open new perspectives to reveal the extraordinary potential of the EVs towards clinical molecular diagnostics.

4. Discussion

In this study, we describe the nickel-based isolation (NBI) as a new approach to selectively enrich heterogeneous (50–700 nm) extracellular vesicles from biological fluids in timely and cost-effective manner. We found that EVs captured through electrostatic interactions can be efficiently dissociated from a nickel-functionalized matrix using chelating agents as excipients, maintaining the properties of a physiological, PBS-like solution in the elution buffer. This aspect is particularly important not only to preserve the integrity of EVs which determines at the end the efficiency in the recovery, but also in view of downstream qualitative and quantitative analyses of the vesicles, as evidenced by

immunocapture-based studies [68,69], or ion-exchange chromatography [28] with a modulation of the ionic strength which can impact fractions of EVs. By contrast, the concentration of EDTA and citric acid could be detrimental for chelating calcium/magnesium ions or cofactors important for cell phenotype/viability or in vitro assays involving the incubation with NBI-isolated EVs. We did not observe variations on the viability (MTT assay) of U87 or colon cancer HCT116 cells exposed for 24 or 48 h to elution buffer 1× or PBS (data not shown). Technically, we present an optimized procedure that can be readily exploited for research in clinical settings and that could be combined with HPLC or size-exclusion procedure to fractionate EVs within the range of 50–800 nm.

The use of an accurate method to isolate vesicles is mandatory for correlation analyses since the assessment of particle distribution can be of relevance for liquid biopsy studies on health and disease states [47]. The quantitative characterization of NBI-isolated EVs from human plasma indicated that polydisperse vesicles can expose surface antigens of different progenitor cells, making difficult any correlation between the vesicle size and the cell of origin. For this reason, we refer to EV lineages indicating all the mixed vesicle populations that are positive to a cell type-distinctive marker and therefore assumed to have a common parental origin. This concept is corroborated by other studies that have investigated the presence or absence of specific antigens on plasma-derived or tumor-derived EVs [56].

The proof-of-principle experiments performed with human plasma including EVs isolated from SK-MEL-28 cells and the melanoma cell-adhesion molecule CD146 demonstrated that different EV lineages are unbiasedly recovered by NBI, resulting to a homogeneous suspension of polydisperse EV lineages. In this context, a targeted immunodepletion of hematopoietic EV lineages in NBI samples can facilitate the discovery and characterization of tumor-derived EV lineages. We have formally proven this possibility by detecting the *BRAF*V600E mutated mRNA, whose copy number was enriched in EVs isolated from plasma of colon cancer patients upon CD235a/CD41a immunodepletion (Fig. 4e and Table S3).

Early detection is a key challenge that could enable specific interventions to reduce patient mortality and morbidity [70]. First, we designed a new ddPCR assay in which the step of RNA extraction can be bypassed, with the important implications of reducing chances of sample contamination, simplifications of the steps towards the results and the sensitivity obtained. In this context, the sensitivity over DNA analysis can be favored by the higher relative number of RNA molecules present in the sample. Second, the advantage of NBI in detecting mutated *BRAF* and *KRAS* transcripts in comparison with CD147-positive EVs and the use of a label-free method can provide better sensitivity for tumor-derived vesicles.

KRAS and *BRAF* are two genes clinically relevant for the prognostic role [71,72], and therapeutic options [73] not only for colon cancer. We have shown that, through liquid biopsy, it is possible to identify fractions of secreted EVs carrying tumor biomarkers with a sensitivity and accuracy that led to re-consider the mutational status in at least 10% of the patients analysed. Currently, the analysis of circulating tumor biomarkers, based on cell-free DNA, shows incomplete sensitivity in lung cancer [74]. In our proof-of-concept study, despite the small number of cases analysed, we reached a complete concordance with the tumor-derived data in detecting *BRAF* and *KRAS* mutations from liquid biopsy. Importantly, some cases showed mutations only in the secreted EVs, suggesting that NBI-ddPCR could serve to infer the presence of specific cell sub-populations hardly detectable in tissue biopsy. This possibility could allow a deeper characterization of tumor heterogeneity and/or its evolution during therapy, with potential impact for the clinical managements of patients. Addressing the low fraction of cells that could generate the EV sub-populations detectable by NBI-ddPCR, systematic studies are needed to understand the threshold specificities and the potential clinical relevance. We believe these findings can relevantly contribute to the rational

establishment of EV-based liquid biopsy studies for the future benefit of clinical diagnostics.

Acknowledgements

We are grateful to Drs. Ilaria Ferlenghi and Fabiola Giusti (SBAD, GSK Vaccines, Siena, Italy) for their assistance in structural microscopy. We thank Dr. D. Di Vizio (Cedars-Sinai Medical Center, USA) for providing suggestions and helpful comments on the manuscript, and Dr. Manuela Basso (CIBIO, University of Trento) for precious discussions on EVs biology.

This research was supported by Associazione Italiana per la Ricerca sul Cancro (to A.P.), Fondazione Cassa di Risparmio Trento e Rovereto (to F.D. and A.Q.), and the Italian Miur (FFABR, to V.G.D.).

Funding sources

Associazione Italiana per la Ricerca sul Cancro (AIRC, N. 21548), Fondazione Cassa di Risparmio Trento e Rovereto (CARITRO), and the Italian Ministero Istruzione, Università e Ricerca (Miur).

Declaration of interests

The authors declare competing interests. The procedure of NBI reported in this manuscript is currently under consideration for patenting.

Author contributions

V.G.D., A.P. and A.Q. conceived NBI, the project and the experimental design. V.G.D. and M.N. optimized the NBI protocol, performed the experiments and analysed the data; M.N. and C.Z. did cell cultures; I.P. performed FACS experiments and qNANO measurements for EV integrity; G.S. performed TEM experiments; C.P., L.L. and C.P. prepared liposomes and performed spectroscopic analyses; A.M. did RNA extraction from EVs; P.P., G.L.M., selected human plasma samples and recorded blood count data; H.B. provided plasma samples of prostate cancer patients and, together with F.D., shared her expertise on prostate cancer markers; L.P. provided plasma samples of colon cancer patients and, together with P.U., performed EasyPCR on FFPE samples; V.G.D., M.N., A.Q., A.P. wrote the manuscript and all the authors revised it.

Appendix A. Supplementary data

Supplementary data to this article can be found online at <https://doi.org/10.1016/j.ebiom.2019.04.039>.

References

- [1] Raposo G, Stoorvogel W. Extracellular vesicles: exosomes, microvesicles, and friends. *J Cell Biol* 2013 Feb 18;200(4):373–83 Internet. cited 2017 Jan 17. Available from <http://www.jcb.org/lookup/doi/10.1083/jcb.201211138>.
- [2] Antonyak MA, Cerione RA. Microvesicles as mediators of intercellular communication in cancer. *Methods Mol Biol* 2014;1165:147–73 Internet. cited 2017 Jan 31. Available from http://link.springer.com/10.1007/978-1-4939-0856-1_11.
- [3] Al-Nedawi K, Meehan B, Micallef J, Lhotak V, May L, Guha A, et al. Intercellular transfer of the oncogenic receptor EGFRvIII by microvesicles derived from tumour cells. *Nat Cell Biol* 2008;10(5):619–24.
- [4] Colombo M, Raposo G, Thery C. Biogenesis, secretion, and intercellular interactions of exosomes and other extracellular vesicles. *Annu Rev Cell Dev Biol* 2014 Oct 11;30(1):255–89 Internet. cited 2017 Jun 27. Available from <http://www.ncbi.nlm.nih.gov/pubmed/25288114>.
- [5] van Niel G, D'Angelo G, Raposo G. Shedding light on the cell biology of extracellular vesicles. *Nat Rev Mol Cell Biol* 2018;19(4):213–28 Internet. Available from <http://www.nature.com/doi/10.1038/nrm.2017.125>.
- [6] Thery C, Amigorena S, Raposo G, Clayton A. Isolation and characterization of exosomes from cell culture supernatants and biological fluids. *Curr Protoc Cell Biol* 2006 Apr. <https://doi.org/10.1002/0471143030.cb0322s30> Internet. [cited 2017 Jan 17];Chapter 3:Unit 3.22. Available from:..
- [7] Tkach M, Thery C. Communication by extracellular vesicles: where we are and where we need to go. *Cell* 2016;164(6):1226–32.

- [8] Nogués L, Benito-Martin A, Hergueta-Redondo M, Peinado H. The influence of tumour-derived extracellular vesicles on local and distal metastatic dissemination. *Mol Aspects Med* 2018;60:15–26.
- [9] Kahler C, Kalluri R. Exosomes in tumor microenvironment influence cancer progression and metastasis. *J Mol Med* 2013;91(4):431–7.
- [10] Yáñez-Mó M, Siljander PR-M, Andreu Z, Zavec AB, Borràs FE, Buzas EI, et al. Biological properties of extracellular vesicles and their physiological functions. *J Extracell Vesicles* 2015;4:27066 Internet. cited 2017 Jan 17. Available from: <http://www.ncbi.nlm.nih.gov/pubmed/25979354>.
- [11] Wiklander OPB, Nordin JZ, O'Loughlin A, Gustafsson Y, Corso G, Mäger I, et al. Extracellular vesicle in vivo biodistribution is determined by cell source, route of administration and targeting. *J Extracell Vesicles* 2015;4 (26316).
- [12] Fais S, O'Driscoll L, Borràs FE, Buzas E, Camussi G, Cappello F, et al. Evidence-based clinical use of nanoscale extracellular vesicles in nanomedicine. *ACS Nano* 2016;10(4):3886–99.
- [13] Chen J, Xu Y, Wang X, Liu D, Yang F, Zhu X, et al. Rapid and efficient isolation and detection of extracellular vesicles from plasma for lung cancer diagnosis. *Lab Chip* 2019;19(3):432–43 Internet. [cited 2019 Jan 11]; Available from: <http://xlink.rsc.org/?DOI=C8LC01193A>.
- [14] Ortega FG, Piguillem SV, Messina GA, Tortella GR, Rubilar O, Jiménez Castillo MI, et al. EGFR detection in extracellular vesicles of breast cancer patients through immunosensor based on silica-chitosan nanopatform. *Talanta* 2019 Mar 1;194:243–52 Internet. cited 2019 Jan 11. Available from: <https://www.sciencedirect.com/science/article/pii/S0039914018310464?via%3DIihub>.
- [15] Lee JS, Hur JY, Kim IA, Kim HJ, Choi CM, Lee JC, et al. Liquid biopsy using the supernatant of a pleural effusion for EGFR genotyping in pulmonary adenocarcinoma patients: a comparison between cell-free DNA and extracellular vesicle-derived DNA. *BMC Cancer* 2018 Dec 10;18(1):1236 Internet. cited 2019 Jan 11. Available from: <https://bmccancer.biomedcentral.com/articles/10.1186/s12885-018-5138-3>.
- [16] Yang S, Che SPY, Kurywchak P, Tavormina JL, Gansmo LB, Correa de Sampaio P, et al. Detection of mutant KRAS and TP53 DNA in circulating exosomes from healthy individuals and patients with pancreatic cancer. *Cancer Biol Ther* 2017 Mar 4;18(3):158–65 Internet. cited 2019 Jan 11. Available from: <https://www.tandfonline.com/doi/full/10.1080/15384047.2017.1281499>.
- [17] Allenson K, Castillo J, San Lucas FA, Scelo G, Kim DU, Bernard V, et al. High prevalence of mutant KRAS in circulating exosome-derived DNA from early-stage pancreatic cancer patients. *Ann Oncol* 2017;28(4):741–7.
- [18] Vagner T, Spinelli C, Minciacci VR, Balaj L, Zandian M, Conley A, et al. Large extracellular vesicles carry most of the tumour DNA circulating in prostate cancer patient plasma. *J Extracell Vesicles* 2018 Dec 7;7(1):1505403 Internet. cited 2019 Jan 11. Available from: <https://www.tandfonline.com/doi/full/10.1080/20013078.2018.1505403>.
- [19] EV-TRACK Consortium J, Van Deun J, Mestdagh P, Agostinis P, Akay Ö, Anand S, et al. EV-TRACK: transparent reporting and centralizing knowledge in extracellular vesicle research. *Nat Methods* 2017 Feb 28;14(3):228–32 Internet. cited 2017 May 18. Available from: <http://www.nature.com/doi/full/10.1038/nmeth.4185>.
- [20] Gardiner C, Di Vizio D, Sahoo S, Théry C, Witwer KW, Wauben M, et al. Techniques used for the isolation and characterization of extracellular vesicles: results of a worldwide survey. *J Extracell Vesicles* 2016 Oct 31;5(0) Internet. cited 2017 Jan 17. Available from: <http://www.journalofextracellularvesicles.net/index.php/jev/article/view/32945>.
- [21] Momen-Heravi F, Balaj L, Alian S, Mantel P-Y, Halleck AE, Trachtenberg AJ, et al. Current methods for the isolation of extracellular vesicles. *Biol Chem* 2013 Jan 1;394(10):1253–62 Internet. cited 2017 Jan 17. Available from: <http://www.ncbi.nlm.nih.gov/pubmed/23770532>.
- [22] Cvjetkovic A, Lötvall J, Lässer C. The influence of rotor type and centrifugation time on the yield and purity of extracellular vesicles. *J Extracell Vesicles* 2014 Jan 24;3(1):23111 Internet. cited 2017 May 18. Available from: <https://www.tandfonline.com/doi/full/10.3402/jev.v3.23111>.
- [23] Liang K, Liu F, Fan J, Sun D, Liu C, Lyon CJ, et al. Nanoplasmonic quantification of tumour-derived extracellular vesicles in plasma microsomes for diagnosis and treatment monitoring. *Nat Biomed Eng* 2017 (pii: 0021).
- [24] Wan Y, Cheng C, Liu X, Hao SJ, Nisic M, Zhu CD, et al. Rapid magnetic isolation of extracellular vesicles via lipid-based nanopores. *Nat Biomed Eng* 2017 (pii: 0058).
- [25] Oliveira-Rodríguez M, López-Cobo S, Reyburn HT, Costa-García A, López-Martín S, Yáñez-Mó M, et al. Development of a rapid lateral flow immunoassay test for detection of exosomes previously enriched from cell culture medium and body fluids. *J Extracell Vesicles* 2016;5:31803.
- [26] Deregibus MC, Figliolini F, D'Antico S, Manzini PM, Pasquino C, De Lena M, et al. Charge-based precipitation of extracellular vesicles. *Int J Mol Med* 2016 Nov 29;38(5):1359–66 Internet. cited 2017 Jan 17. Available from: <http://www.spandidos-publications.com/10.3892/ijmm.2016.2759>.
- [27] Kosanović M, Milutinović B, Goč S, Mitić N, Janković M. Ion-exchange chromatography purification of extracellular vesicles. *Biotechniques* 2017;63(2):65–71.
- [28] Heath N, Grant L, De Oliveira TM, Rowlinson R, Osteikoetxea X, Dekker N, et al. Rapid isolation and enrichment of extracellular vesicle preparations using anion exchange chromatography. *Sci Rep* 2018 Dec 10;8(1):5730 Internet. cited 2019 Jan 11. Available from: <http://www.ncbi.nlm.nih.gov/pubmed/29636530>.
- [29] Předota M, Machesky ML, Wesolowski DJ. Molecular origins of the zeta potential. *Langmuir* 2016;32(40):10189–98.
- [30] Salgin S, Salgin U, Bahadır S. Zeta potentials and isoelectric points of biomolecules: the effects of ion types and ionic strengths. *Int J Electrochem Sci* 2012;7(12):12404–14.
- [31] Kaszuba M, Corbett J, Watson FM, Jones A. High-concentration zeta potential measurements using light-scattering techniques. *Philos Trans R Soc A Math Phys Eng Sci* 2010;368(1927):4439–51.
- [32] Vogel R, Pal AK, Jambhrunkar S, Patel P, Thakur SS, Reátegui E, et al. High-resolution single particle zeta potential characterisation of biological nanoparticles using tunable resistive pulse sensing. *Sci Rep* 2017;7(1):17479.
- [33] Rupert DLM, Claudio V, Lässer C, Bally M. Methods for the physical characterization and quantification of extracellular vesicles in biological samples. *Biochim Biophys Acta* 2017 Jan;1861(1 Pt A):3164–79 Internet. cited 2017 Jan 17. Available from: <http://linkinghub.elsevier.com/retrieve/pii/S03044116516302756>.
- [34] Di Vizio D, Morello M, Dudley AC, Schow PW, Adam RM, Morley S, et al. Large oncosomes in human prostate cancer tissues and in the circulation of mice with metastatic disease. *Am J Pathol* 2012 Nov;181(5):1573–84 Internet. cited 2017 Jun 27. Available from: <http://www.ncbi.nlm.nih.gov/pubmed/23022210>.
- [35] Van Deun J, Mestdagh P, Sormunen R, Cocquyt V, Vermaelen K, Vandesompele J, et al. The impact of disparate isolation methods for extracellular vesicles on downstream RNA profiling. *J Extracell Vesicles* 2014 Sep 18;3(0) Internet. cited 2017 Jan 17. Available from: <http://www.journalofextracellularvesicles.net/index.php/jev/article/view/24858>.
- [36] D'Agostino VG, Adami V, Provenzani A. A novel high throughput biochemical assay to evaluate the HuR protein-RNA complex formation. *PLoS One* 2013 Jan;8(8):e72426 Internet. cited 2014 Jul 25. Available from: <http://www.pubmedcentral.nih.gov/articlerender.fcgi?artid=3741180&tool=pmcentrez&rendertype=abstract>.
- [37] Xu C, Liu K, Ahmed H, Loppnau P, Schapira M, Min J. Structural basis for the discriminative recognition of N⁶-methyladenosine RNA by the human YT521-B homology domain family of proteins. *J Biol Chem* 2015 Oct 9;290(41):24902–13 Internet. cited 2017 May 25. Available from: <http://www.ncbi.nlm.nih.gov/pubmed/26318451>.
- [38] Llorente A, Skotland T, Sylvänne T, Kauhane D, Róg T, Orłowski A, et al. Molecular lipidomics of exosomes released by PC-3 prostate cancer cells. *Biochim Biophys Acta* 2013 Jul;1831(7):1302–9 Internet. cited 2017 May 25. Available from: <http://www.ncbi.nlm.nih.gov/pubmed/24046871>.
- [39] Haraszti RA, Didiot M-C, Sapp E, Leszyk J, Shaffer SA, Rockwell HE, et al. High-resolution proteomic and lipidomic analysis of exosomes and microvesicles from different cell sources. *J Extracell Vesicles* 2016 Jan 24;5(1):32570 Internet. cited 2017 May 25. Available from: <https://www.tandfonline.com/doi/full/10.3402/jev.v5.32570>.
- [40] MacDonald RC, MacDonald RI, Menco BP, Takeshita K, Subbarao NK, Hu LR. Small-volume extrusion apparatus for preparation of large, unilamellar vesicles. *Biochim Biophys Acta* 1991;1061(2):297–303 Internet. Jan 30 [cited 2017 Jun 27. Available from: <http://www.ncbi.nlm.nih.gov/pubmed/1998698>.
- [41] Vogel R, Coumans FAW, Maltesen RG, Böing AN, Bonnington KE, Broekman ML, et al. A standardized method to determine the concentration of extracellular vesicles using tunable resistive pulse sensing. *J Extracell Vesicles* 2016 Jan 24;5(1):31242 Internet. cited 2017 May 18. Available from: <https://www.tandfonline.com/doi/full/10.3402/jev.v5.31242>.
- [42] Colombo M, Moita C, van Niel G, Kowal J, Vigneron J, Benaroch P, et al. Analysis of ESCRT functions in exosome biogenesis, composition and secretion highlights the heterogeneity of extracellular vesicles. *J Cell Sci* 2013 Dec 15;126(24):5553–65 Internet. cited 2017 Jun 27. Available from: <http://www.ncbi.nlm.nih.gov/pubmed/24105262>.
- [43] Meister M, Tikkanen R. Endocytic trafficking of membrane-bound cargo: a flotillin point of view. *Membranes (Basel)* 2014 Jul 11;4(3):356–71 Internet. cited 2019 Jan 14. Available from: <http://www.ncbi.nlm.nih.gov/pubmed/25019426>.
- [44] Yuana Y, Böing AN, Grootemaat AE, van der Pol E, Hau CM, Cizmar P, et al. Handling and storage of human body fluids for analysis of extracellular vesicles. *J Extracell Vesicles* 2015;4:29260.
- [45] Wei Z, Batagov AO, Carter DRF, Krichevsky AM. Fetal bovine serum RNA interferes with the cell culture derived extracellular RNA. *Sci Rep* 2016 Aug 9;6(1):31175 Internet. cited 2017 May 18. Available from: <http://www.nature.com/articles/srep31175>.
- [46] Abels ER, Breakefield XO. Introduction to extracellular vesicles: biogenesis, RNA cargo selection, content, release, and uptake. *Cell Mol Neurobiol* 2016 Apr 6;36(3):301–12 Internet. cited 2017 May 18. Available from: <http://link.springer.com/10.1007/s10571-016-0366-z>.
- [47] Nomura S. Extracellular vesicles and blood diseases. *Int J Hematol* 2017 Apr 27;105(4):392–405 Internet. cited 2017 May 18. Available from: <http://link.springer.com/10.1007/s12185-017-2180-x>.
- [48] Wolf P. The nature and significance of platelet products in human plasma. *Br J Haematol* 1967;13(3):269–88.
- [49] Wisgrill L, Lamm C, Hartmann J, Preißing F, Dragosits K, Bee A, et al. Peripheral blood microvesicles secretion is influenced by storage time, temperature, and anticoagulants. *Cytom Part A* 2016 Jul;89(7):663–72 Internet. cited 2019 Jan 14. Available from: <http://www.ncbi.nlm.nih.gov/pubmed/27442840>.
- [50] Valkonen S, van der Pol E, Böing A, Yuana Y, Yliperttula M, Nieuwland R, et al. Biological reference materials for extracellular vesicle studies. *Eur J Pharm Sci* 2017 Feb 15;98:4–16 Internet. cited 2017 May 18. Available from: <http://linkinghub.elsevier.com/retrieve/pii/S0928098716303578>.
- [51] Vagida M, Arakelyan A, Lebedeva A, Grivel J-C, Shpektor A, Vasilieva E, et al. Flow analysis of individual blood extracellular vesicles in acute coronary syndrome. *Platelets* 2017 Mar 17;28(2):165–73 Internet. cited 2017 May 18. Available from: <https://www.tandfonline.com/doi/full/10.1080/09537104.2016.1212002>.
- [52] Melki I, Tessandier N, Zufferey A, Boilard E. Platelet microvesicles in health and disease. *Platelets* 2017;28(3):214–21.
- [53] Aatonen MT, Ohman T, Nyman TA, Laitinen S, Grönholm M, Siljander PR-M. Isolation and characterization of platelet-derived extracellular vesicles. *J Extracell Vesicles* 2014;3 Internet. cited 2017 Feb 8. Available from: <http://www.ncbi.nlm.nih.gov/pubmed/25147646>.
- [54] Woodford-Thomas T, Thomas ML. The leukocyte common antigen, CD45 and other protein tyrosine phosphatases in hematopoietic cells. *Semin Cell Biol* 1993 Dec;4(6):

- 409–37 Internet. cited 2017 Jul 31. Available from <http://www.ncbi.nlm.nih.gov/pubmed/8305680>.
- [55] Cardi G, Mastrangelo MJ, Berd D. Depletion of T-cells with the CD4+CD45R+ phenotype in lymphocytes that infiltrate subcutaneous metastases of human melanoma. *Cancer Res* 1989 Dec 1;49(23):6562–5 Internet. cited 2017 Jul 31. Available from: <http://www.ncbi.nlm.nih.gov/pubmed/2479465>.
- [56] Belov L, Matic KJ, Hallal S, Best OG, Mulligan SP, Christopherson RI. Extensive surface protein profiles of extracellular vesicles from cancer cells may provide diagnostic signatures from blood samples. *J Extracell Vesicles* 2016;5:25355 Internet. cited 2017 Aug 1. Available from <http://www.ncbi.nlm.nih.gov/pubmed/27086589>.
- [57] Yoshioka Y, Kosaka N, Konishi Y, Ohta H, Okamoto H, Sonoda H, et al. Ultra-sensitive liquid biopsy of circulating extracellular vesicles using ExoScreen. *Nat Commun* 2014;5:3591.
- [58] Smith ZJ, Lee C, Rojalin T, Carney RP, Hazari S, Knudson A, et al. Single exosome study reveals subpopulations distributed among cell lines with variability related to membrane content. *J Extracell Vesicles* 2015;4:28533.
- [59] Jeppesen DK, Hvam ML, Primdahl-Bengtson B, Boysen AT, Whitehead B, Dyrskjöld L, et al. Comparative analysis of discrete exosome fractions obtained by differential centrifugation. *J Extracell Vesicles* 2014;3:25011.
- [60] Yoshioka Y, Konishi Y, Kosaka N, Katsuda T, Kato T, Ochiya T. Comparative marker analysis of extracellular vesicles in different human cancer types. *J Extracell Vesicles* 2013;2.
- [61] Tatischeff I. Innovative approach of prostate cancer by the way of tumour cell-derived extracellular vesicles. *J Extracell Vesicles* 2016. <https://doi.org/10.0.13.74/jev.v5.31552>.
- [62] Chen WW, Balaj L, Liao LM, Samuels ML, Kotsopoulos SK, Maguire CA, et al. Beaming and droplet digital pcr analysis of mutant idh1 mrna in glioma patient serum and cerebrospinal fluid extracellular vesicles. *Mol Ther Nucleic Acids* 2013;2 (e109).
- [63] McDonald B, Reep B, Lapetina EG, Molina y Vedia L. Glyceraldehyde-3-phosphate dehydrogenase is required for the transport of nitric oxide in platelets. *Proc Natl Acad Sci U S A* 1993 Dec 1;90(23):11122–6 Internet. cited 2017 May 18. Available from <http://www.ncbi.nlm.nih.gov/pubmed/7902582>.
- [64] Ulivi P, Scarpi E, Passardi A, Marisi G, Calistri D, Zoli W, et al. eNOS polymorphisms as predictors of efficacy of bevacizumab-based chemotherapy in metastatic colorectal cancer: data from a randomized clinical trial. *J Transl Med* 2015;13:258.
- [65] Marisi G, Scarpi E, Passardi A, Nanni O, Ragazzini A, Valgiusti M, et al. Circulating VEGF and eNOS variations as predictors of outcome in metastatic colorectal cancer patients receiving bevacizumab. *Sci Rep* 2017;7(1):1293.
- [66] Tian Y, Ma L, Gong M, Su G, Zhu S, Zhang W, et al. Protein profiling and sizing of extracellular vesicles from colorectal cancer patients via flow cytometry. *ACS Nano* 2018;12(1):671–80.
- [67] Ramakrishnaiah V, Thumann C, Fofana I, Habersetzer F, Pan Q, de Ruiter PE, et al. Exosome-mediated transmission of hepatitis C virus between human hepatoma Huh7.5 cells. *Proc Natl Acad Sci* 2013;110(32):13109–13.
- [68] Nakai W, Yoshida T, Diez D, Miyatake Y, Nishibu T, Imawaka N, et al. A novel affinity-based method for the isolation of highly purified extracellular vesicles. *Sci Rep* 2016 Sep 23;6:33935 Internet. cited 2017 Jan 17. Available from: <http://www.nature.com/articles/srep33935>.
- [69] Kim D, Nishida H, An SY, Shetty AK, Bartosh TJ, Prockop DJ. Chromatographically isolated CD63+CD81+ extracellular vesicles from mesenchymal stromal cells rescue cognitive impairments after TBI. *Proc Natl Acad Sci U S A* 2016 Jan 5;113(1):170–5 Internet. cited 2019 Jan 14. Available from <http://www.pnas.org/lookup/doi/10.1073/pnas.1522297113>.
- [70] Srinivas PR, Kramer BS, Srivastava S. Trends in biomarker research for cancer detection. *Lancet Oncol* 2001;2(11):698–704.
- [71] Phipps AI, Limburg PJ, Baron JA, Burnett-Hartman AN, Weisenberger DJ, Laird PW, et al. Association between molecular subtypes of colorectal cancer and patient survival. *Gastroenterology* 2015;148(1) (77-87.e2).
- [72] Thomsen M, Skovlund E, Sorbye H, Bolstad N, Nustad KJ, Glimelius B, et al. Prognostic role of carcinoembryonic antigen and carbohydrate antigen 19-9 in metastatic colorectal cancer : a BRAF -mutant subset with high CA 19-9 level and poor outcome. *Br J Cancer* 2018. <https://doi.org/10.1038/s41416-018-0115-9> Internet. (March). Available from:.
- [73] El-Deiry WS, Vijayvergia N, Xiu J, Scicchitano A, Lim B, Yee NS, et al. Molecular profiling of 6,892 colorectal cancer samples suggests different possible treatment options specific to metastatic sites. *Cancer Biol Ther* 2015;16(12):1726–37.
- [74] Rolfo C, Mack PC, Scagliotti GV, Baas P, Barlesi F, Bivona TG, et al. IASLC statement paper: liquid biopsy for advanced non-small cell lung cancer (NSCLC). *J Thorac Oncol* 2018;13(9):1248–68.